Energy Conversion and Management 105 (2015) 782–790

Contents lists available at ScienceDirect

Energy Conversion and Management

journal homepage: www.elsevier.com/locate/enconman

Evaluation of optimal dual axis concentrated photovoltaic thermal system with active ventilation using Frog Leap algorithm

H. Gholami [a], A.I. Sarwat [b], H. Hosseinian [a], A. Khalilnejad [b,*]

[a] Electrical Engineering Department, Amirkabir University of Technology (AUT), Tehran, Iran
[b] Electrical Engineering Department, Center of Energy, Power & Sustainability (EPS), Florida International University (FIU), Miami, USA

ARTICLE INFO

Article history:
Received 13 April 2015
Accepted 11 August 2015
Available online 27 August 2015

Keywords:
CPVT system
Triple-junction cell
Frog Leap algorithm
Solar tracker
Active ventilation

ABSTRACT

In this study, design and optimization of a concentrated photovoltaic thermal (CPVT) system considering electrical, mechanical, and economical aspects is investigated. For this purpose, each section of the system is simulated in MATLAB, in detail. Triple-junction photovoltaic cells, which are the most recent technology, are used in this study. They are more efficient in comparison to conventional photovoltaic cells. Unlike ordinary procedures, in this work active ventilation is used for absorbing the thermal power of radiation, using heat storage tanks, which not only results in increasing the electrical efficiency of the system through decreasing the temperature, but also leads to storing and managing produced thermal energy and increasing the total efficiency of the system up to 85 percent. The operation of the CPVT system is investigated for total hours of the year, considering the needed thermal load, meteorological conditions, and hourly radiation of Khuznin, a city in Qazvin province, Iran. Finally, the collector used for this system is optimized economically, using frog leap algorithm, which resulted in the cost of 13.4 $/m^2 for a collector with the optimal distance between tubes of 6.34 cm.

1. Introduction

In recent years, the concentrated photovoltaic thermal (CPVT) systems have been rapidly developed [1,2]. In these systems, the radiation is transmitted to cells, using reflectors. With this method, the incident radiation to the cells increases significantly [3–8]. The CPV consists of three parts including the absorber, concentrator, and solar radiation tracker. The absorber consists of the solar cell part and the thermal ventilation system. The concentrator focuses the radiation to the absorber. As the CPV works with the beam radiation, the absorber and concentrator should follow the position of the sun to maximize the incident beam radiation. In order to concentrate the radiation, two major technologies of Fresnel lens [9,10] and parabolic concentrators [11] can be used. Plus, in recent years, triple-junction solar cells have been widely investigated. In these systems, when increasing the current, the voltage increases in logarithmic scale [12]. Also, they are less affected by temperature variation in comparison with silicon based samples [9]. Based on the level of concentration, there are three major concentrators with low, medium, and high rate of concentration. In a study in 2010, a solar system with low rate of concentration is discussed. The model was used to perform a sensitivity analysis in order to highlight the relevance of the leading working parameters (such as irradiance) in system performance [13]. In 2011, instead of implementation of conventional cells, the usage of cells with efficient operation such as GaAs with a linear concentrator is investigated [14]. In another study in 2011, a case study in Sweden, a low concentrating CPVT system is performed and a complete methodology to characterize, simulate, and evaluate concentrating photovoltaic/thermal hybrids is proposed [15]. In 2012, the operation of single and double-axis solar tracker system installed on the roof of a building is analyzed [16].

The obtained thermal power can be used for both heating and cooling purposes which are described in recent studies [17,18]. In 2013, performance analysis of a novel concentrating photovoltaic combined system is performed. Also, energy and exergy analyses of the system is evaluated, economical analysis is performed, and the experimental results are compared to data obtained by the control system [19]. In 2014, the optical performance of a CPVT system is evaluated. The theoretical model of the optical performance of the system under real application condition was established and the outdoor experiment was carried out to compare the simulation evaluation [20]. In 2015, parametric performance analysis of a concentrated photovoltaic co-generation system equipped with a thermal storage tank is done. The system utilized dual-axis tracker

* Corresponding author. Tel.: +98 914 915 6215.
E-mail address: akhal026@fiu.edu (A. Khalilnejad).

http://dx.doi.org/10.1016/j.enconman.2015.08.033
0196-8904/

and multiple solar energy collector (SEC) modules and a forced cooling system [21]. In another study in 2015, analysis of U-shaped solar energy collector of a CPVT system is evaluated, numerically and experimentally [22].

In the previous studies, the optimization of an active ventilation system of the concentrated solar collectors, considering hourly operation of the CPVT system for a long term period, has not been performed. The optimal dimensions of the thermal absorbing system and its economical aspects are discussed in this work.

So, in this study, with a dual axis tracker and open-loop controller, the operation of a concentrated PVT system is investigated. The electrical and thermal characteristics of the system are discussed with the simulation of a detailed model of the system. Also, meteorological conditions such as wind speed, ambient temperature, clearness index, and solar radiation are considered in the operation of the system. For using the heat absorbed by the collector, active ventilation using a heat storage tank is used. Also, the economic optimization of the system is performed, using Frog Leap algorithm. Fig. 1. shows the schematic of the system.

As it can be seen in Fig. 10, the water is delivered to the tubes of the collector by the pumps. So, the temperature of the water inside the tube increases and the water returns back to the tank. This cycle lasts as long as the radiation is available. The tank contains an outlet for heat consumption of water, and an inlet for getting the cold water.

2. CPVT system

2.1. Solar trackers

A solar tracker is a device that changes the position of the solar module so that that the radiation can be perpendicular to the surface. In the design of the solar tracker, the position of the sun and the earth in a year period should be evaluated.

Based on the number of their axis, the radiation tracking systems are known as single or dual axis trackers [23]. Their actuation systems have two types of actuators: active and passive [24]. These methods, which are both open-loop or close loop, are different from each other in several aspects such as accuracy, pace, power consumption, reflection to the various meteorological conditions, need for maintenance, and cost [25].

2.2. Reflectors

The conventional material for reflectors is Anodized Aluminum. However, one of the disadvantages of this is that when a large reflector is constructed, the aluminum structure begins to deviate from its main characteristic which causes a depression in the surface of the reflector. So, undesired reflections are produced which leads to optical loss and reduction of efficiency. Another issue of anodized aluminum is that in working conditions with high temperatures, the amount of depression increases drastically.

Recently, Aluminum-Polymer-Laminated Steel is used to avoid these issues in Aluminum reflectors. The characteristics are discussed by Borgen [26]. The steel used in this compound makes it tighter which solves the depression problem occurring in high temperatures.

2.3. Triple-junction cells

Multi-junction PV cells have been proven to be particularly well suited for a concentrating system where sunlight can be focused through lenses or mirrors into a much smaller cell [27]. The V–I characteristic of the solar cell is described as [28]:

$$I = -I_{SAT}\left[\exp\left(\frac{q(V+IR_s)}{nkT}\right) - 1\right] + I_L \tag{1}$$

where I_{sat} is reverse saturation current, V is cell voltage, R_s is series resistance, n is ideality factor of a diode, which is a measure of how closely the diode follows the ideal diode equation, k is Boltzmann constant, T is cell temperature, and I_L is light generated current. I_{sat} and I_L can be described as:

$$\begin{aligned} I_{SAT} &= J_{SAT}A_A \\ I_L &= J_L A_A \\ J_L &= RW_R \end{aligned} \tag{2}$$

where J is the current density, A_A is aperture area, R is the responsivity described as the ratio between the current from the illuminated diode and the incident light power, and W_R is the incident solar radiation intensity to the surface.

The direction of current is the opposite of the direction of a common diode. If R_s be a non-zero quantity, Eq. (1) should be solved, repetitively. The result of simulation shows that for

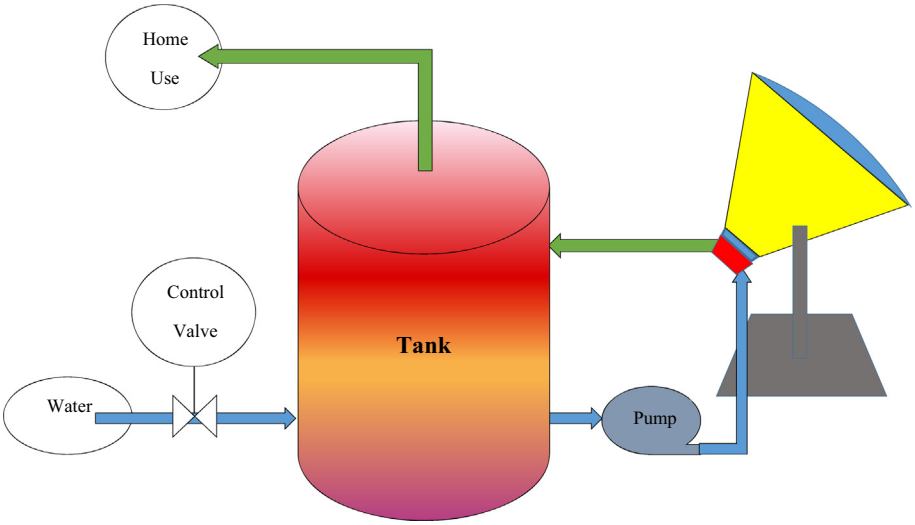

Fig. 1. The schematic of CPV system with active ventilation.

congruity of the data, the series resistance should be dependent of absorbed power by the cell, shown in the following equation:

$$R_S = R_{S0}/X^K + R_{S\infty} \tag{3}$$

where R_{s0} is the series resistance at low intensity, X is concentration, $R_{s\infty}$ is the series resistance at high flux, and K is the series resistance intensity coefficient. The Eq. (3) is represented in Fig. 2 [29]. As can be seen the resistance is a function of the number of photons received at the surface. Also, the dependence of the electrical system of photovoltaic cells on the temperature is expressed as [30]:

$$J_{SAT}(T) \sim T^{3+\gamma/2} \exp\left(-\frac{E_g}{kT}\right) \tag{4}$$

where E_g is the effective energy gap. With describing the V–I characteristics, the open circuit voltage and short Circuit current can be obtained as following:

$$\begin{aligned} I_{sc} &= I_L \\ V_{OC} &= \tfrac{kT}{q} \ln\left(\tfrac{I_L}{I_{SAT}} + 1\right) \end{aligned} \tag{5}$$

Also, the maximum voltage and current can be derived from repetitively solving of the following equation which is the derivative of Eq. (1):

$$V_{MP} = \frac{nkT}{q} \ln\left(\frac{I_L}{I_{SAT}} - \frac{I_{MP}}{I_{SAT}} + 1\right) - I_{MP}R_S \tag{6}$$

So, the efficiency and fill factor (FF) is given in the following equations:

$$FF = \frac{I_{MP}V_{MP}}{I_{sc}V_{OC}} \tag{7}$$

$$\eta = \frac{I_{MP}V_{MP}}{WA_A} \tag{8}$$

where W is the incident solar radiation intensity. According to the mentioned equations, the electrical section of the system is simulated. The parameters needed for simulation are given in Table 1 which is a sample constructed in Spectrolab Inc., a wholly owned subsidiary of The Boeing Company [29,31].

The efficiency and fill factor is shown in Fig. 3. As can be seen, the efficiency is almost constant when the concentration ratio rises. However, the fill factor decreases, gradually, leading to less power production.

2.4. Ventilation

Two major procedures of ventilation of solar collectors are active ventilation and passive ventilation. With passive ventilation, the heat generated in the surface of the collector is transmitted to the air by heat sink. With active ventilation, the heat can be used

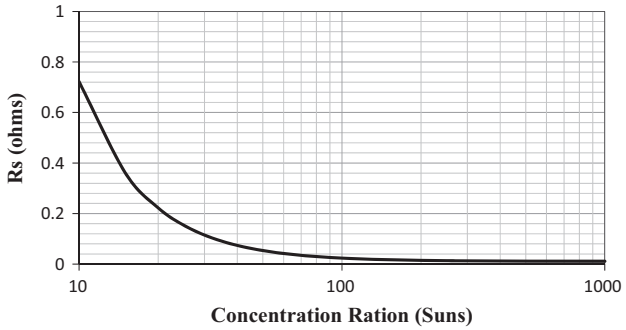

Fig. 2. The series resistance of the cell.

Table 1
Parameters of the cell.

Symbol	Value	Unit
J_{SAT}	$1.01(10^{-20})$ at 25 °C	A/cm^2
A_A	0.27	C m^2
n	2.44	–
i	1.6×10^{-19}	C
	1	eV
K	8.62×10^{-5}	eV/K
$R_{S\infty}$	0.011	Ω
R_{S0}	40	Ω
K	1.75	–
W	0.0901	W/cm^2
W_R	0.139	A/W
E_g	1.6	eV
Γ	1	–

for cooling or heating purposes. So, active ventilation converts a CPV system to a CPVT system. The heat can be produced by convection or radiation. When the heat balance is confirmed, the following equation can be derived for concentrated solar cells [32]:

$$A_c.S - A_c \cdot S \cdot \eta - A_{HS} \cdot \varepsilon \cdot \sigma(T^4 - T_a^4) - A_{HS}h_c(T - T_a) = 0 \tag{9}$$

where A_c is the area of the cell, S is the solar power received to the surface of cell, η is the electrical efficiency, A_{HS} is the area of heat storage tank, ε emitting coefficient, σ is Estefan–Boltzmann constant, h_c is the convection coefficient, T is the cell temperature, and T_a is the ambient temperature.

As shown in Fig. 4, if a heat storage tank is not used, the temperature of the surface of the cells raises drastically. For example, for a concentration rate of 500, the temperature reaches up to 1000 K.

The effect of the heat storage tank on the temperature of cells is shown in Fig. 5. As it can be seen, the temperature decreases significantly due to absorbing of the heat by the fluid inside the tubes.

The energy loss from the collector is obtained from [33]:

$$Q_{loss} = \frac{T_p - T_a}{R_L} = U_L A_c (T_P - T_a) \tag{10}$$

where U_L is the total heat loss coefficient, and T_P is the collector's temperature. U_L can be expressed as:

$$U_L = U_t + U_b + U_e \tag{11}$$

where U_t, U_b, and U_e are the heat loss coefficients of top, bottom, and edges of the collector, respectively.

The heat loss from the top of the collector is due to radiation and convection. Convection and radiation loss coefficients are described as:

$$h_c = \frac{8.6V^{0.6}}{L^{0.4}} \tag{12}$$

$$h_r = \varepsilon\sigma(T_P^2 + T_a^2)(T_P + T_a) \tag{13}$$

where V is the wind speed and L is the length of the collector. So,

$$U_t = h_c + h_r \tag{14}$$

The heat loss coefficients of bottom and edges of the collector are derived from:

$$U_b = \frac{k_b}{t_b} \tag{15}$$

$$U_e = \frac{k_e}{t_e} \tag{16}$$

where t and k are thickness of the tube and the conductance coefficient, respectively. Fig. 6 shows the thermal system representing

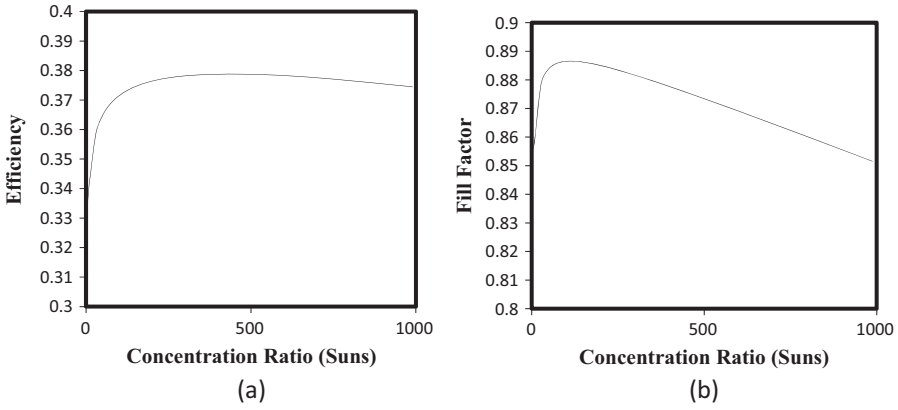

Fig. 3. Efficiency (a) and Fill Factor (b) of cells.

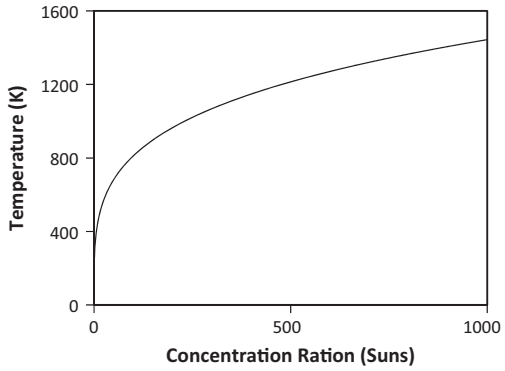

Fig. 4. The temperature of the concentrated cell without using heat storage tank.

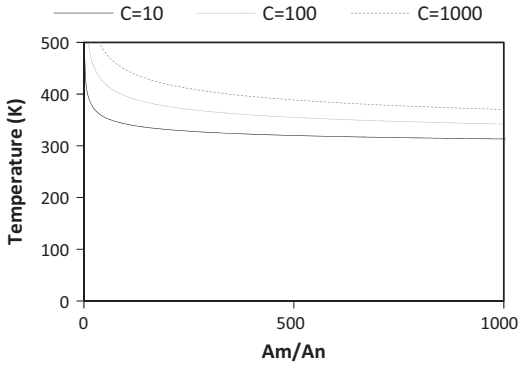

Fig. 5. The dependence of cells temperature to the rate of area of the heat storage tank to the area of collectors surface.

the important dimensions of the collector. For better performance of the system, these parameters should be determined.

The corrected fin efficiency of the collector is expressed by:

$$F' = \frac{\frac{1}{U_L}}{W\left[\frac{1}{U_L(D+(W-D)F)}\right] + \frac{1}{C_b} + \frac{1}{\pi D_i h_{fi}}} \tag{17}$$

where h_{fi} is the forced convection heat transfer coefficient inside the cooling passage. C_b is the conductance of the connection point of the tube and the collector, W is the distance between adjacent tubes, D is the diameter of outer edge of the tubes, D_i is the diameter of the inner edges of the tubes, and F is the efficiency coefficient of the finned area. F can be derived from the following equation:

$$F = \frac{\tan h\left(m\frac{W-D}{2}\right)}{\left(m\frac{W-D}{2}\right)} \tag{18}$$

The coefficient (m) is a term which accounts for the thermal conductivity of the absorber and PV cell and fin thickness is represented by the next equation:

$$m = \sqrt{\frac{U_L}{k\delta}} \tag{19}$$

C_b can be obtained using the heat conductance coefficient (k_b), the average of thickness of connection point (y_b), and the width of the connection point (b), as following:

$$C_b = \frac{k_b b}{y_b} \tag{20}$$

The convection coefficient of the fluid can be derived from [34]:

$$h = \frac{Nuk}{D} \tag{21}$$

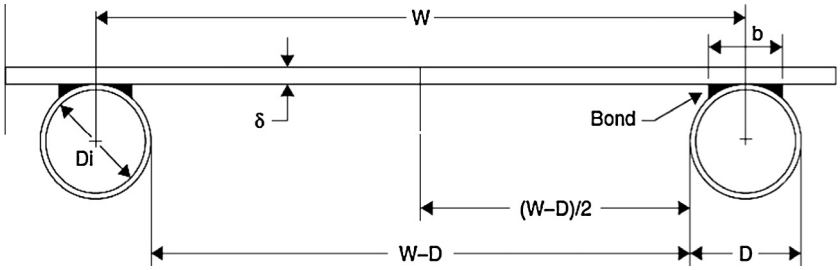

Fig. 6. The schematic of collector and tubes.

Table 2
The constants value in Eq. (22) [33].

Pr	a	b	m	n
0.7	0.00398	0.0114	1.66	1.12
10	0.00236	0.00857	1.66	1.13
∞	0.00172	0.00281	1.66	1.29

where D, k, and Nu are the radius of the tube, the heat conductance coefficient, and Nusselt number, respectively. Nu can be derived from:

$$Nu = Nu_{\infty} + \frac{aw^m}{1+bw^n}$$
$$w = \frac{\mathrm{RePr}D}{L} \tag{22}$$

where Re, Pr, and L are Reynolds number, Prandtl number, and length of collector, respectively. Re is expressed by:

$$\mathrm{Re} = \frac{4\dot{m}}{\pi D\mu} \tag{23}$$

where $\dot{m}$ and μ are density and viscosity of the fluid, respectively. The values of a, b, m, n and, Nu_{∞} are given in Table 2.

The heat removal efficiency factor is given in the following equation:

$$F_R = \frac{\dot{m}C_P}{A_cU_L}\left[1 - \exp\left(-\frac{A_cU_LF'}{\dot{m}C_p}\right)\right] \tag{24}$$

This coefficient is the ration of obtained energy in a practical situation to the obtained energy when the temperature of the cell is equal to the temperature of the fluid. C_p is the specific heat of the collector cooling medium. So, the absorbed heat by the fluid can be derived from the following equation:

$$Q_u = A_cF_R(S - U_L(T_i - T_a)) \tag{25}$$

where T_i is the cooling medium inlet temperature. The thermal efficiency is given by

$$\eta_{th} = \frac{Q_u}{S} \tag{26}$$

The temperature of the surface of the collector is given by the following equation

$$T_p = T_i + \frac{Q_u}{A_cF_RU_L}(1 - F_R) \tag{27}$$

Also, fin thickness, which is an important factor in the designing of the system, is given by [35]

$$\delta = \frac{\frac{\frac{j_o(W-bW^{1/4}-t)^2}{W-bW^{1/4}-t}}{\frac{1}{1-bW^{1/4}-t}-1}}{k}\left[\frac{U_L}{\frac{1}{F'U_LW}-p}\right] \tag{28}$$

where

$$j_o = \frac{U_L}{12}$$
$$p = \frac{1}{\pi h_{fi}D_i} \tag{29}$$

3. Simulation of the system

With active ventilation, the CPV system is converted to a combined heat and power (CHP) system. Fig. 7, represents the flowchart of calculations process of the system.

If the radiation is available, the temperature rises drastically, and with using temperature sensor the pumps start to work and the whole system calculations are performed. Otherwise, just the heat storage tank's calculations are done. The tank is insulated

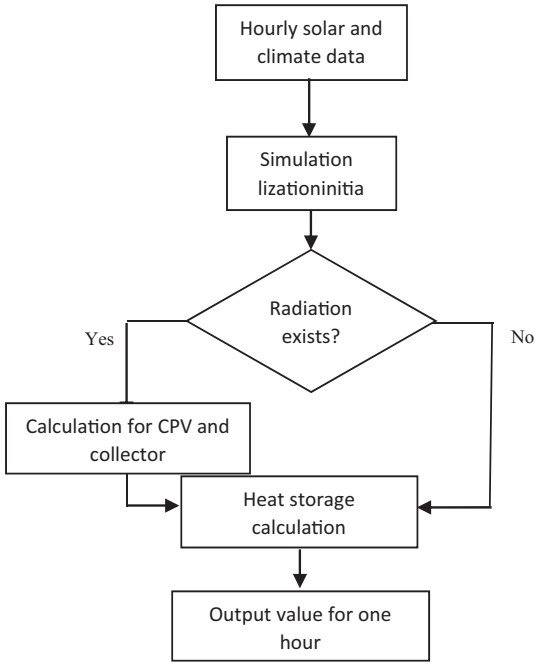

Fig. 7. Flowchart of calculation process.

and the heat capacity of it is 16 (KW/K m^2) [36]. Before the calculation process, the different kinds of energy stored in the tank can be mentioned as following:

- $E_{tank,i}$: the stored energy in the tank and it is equal to:

$$E_{\tan k} = m_{\tan k}c_p(T_{\tan k} - T_a) \tag{30}$$

where m_{tank} is the mass of water inside the tank, and T_{tank} is the temperature of it.

- E_{in}: the inlet energy to the tank from the ventilation system, which is equal to:

$$E_{in} = Q_u \tag{31}$$

- $E_{citywater}$: the inlet energy to the tank from the inlet water, described as following:

$$E_{citywater} = m_{in}c_p(T_a - T_0) \tag{32}$$

where m_{in} is the mass of inlet water and T_0 is the reference temperature.

- E_{use}: the consumed energy due to outflow of the warm water from the tank for heating purposes, which is expressed as:

$$E_{use} = m_{use}c_p(T_{\tan k} - T_0) \tag{33}$$

Where m_{use} is the mass of outlet water.

- E_{loss}: the loss energy from the walls of the tank, which is described as the following equation:

$$E_{loss} = A_{\tan k}R_{\tan k}(T_{\tan k} - T_{air}) \tag{34}$$

where R_{tank} is the heat capacity of the tank. Also, A_{tank} is the area of walls of the heat storage tank.

For the calculation of the energy of the tank, there should be energy balance between the mentioned energies, as following:

$$E_{\tan k,i} = E_{\tan k,i-1} + E_{in,i} + E_{citywater,i} - E_{use,i} - E_{loss,i} \tag{35}$$

where i index represents each hour of the system's operation. T_{tank} can be derived from the following equation:

$$T_{\tan k} = (E_{\tan k}/(m_{\tan k} \cdot c_p)) + T_0 \tag{36}$$

3.1. Radiation and meteorological data

The meteorological data of the location in which the system is simulated and analyzed is based on Khuznin, a city in Qazvin province, Iran. This city has a longitude of 35.861° and a latitude of 49.758° with clean and mild climatic conditions [36]. The hourly radiation for a year depends on various factors such as the number of bright hours of the day, the clearness index, the ambient temperature, the latitude of the region, and the view factor of the sky to ground. The radiation calculation process is described in our previous study [36]. The equation of total hourly radiation is expressed as:

$$I_T = I_b R_b + I_{d,iso} F_{c-s} + I_{d,cs} R_b + I_{d,Hz} F_{c-Hz} + I_g F_{c-g} \quad (37)$$

where I_b is the incident beam radiation, R_b is the geometric factor defined as the ratio of the beam radiation on tilted surface to that on horizontal surface at any time, i_d is the diffused incident radiation, I_g is the reflected radiation, and F is the view factor of the surface to sky and ground.

Fig. 8a shows the total and beam hourly radiation for a dual axis solar tracker. The ratio of total and beam radiation for a collector with a dual axis tracker to a fixed collector with optimal surface angle of 38° is 1.34 and 1.65, respectively. Fig. 8b, shows the incident radiation fractions to the surface of a dual axis collector for the first day of the year. The total energy received at the surface is 15.95 MJ/m^2 with 70.52, 19.84, and 9.64 percent for beam, diffused, and reflected radiation, respectively. Also, the hourly wind speed data for the region is shown in Fig. 9. The average wind speed is 4.87 m/s.

3.2. Optimization of the system using frog leap algorithm

The frog leap is an algorithm taken from nature. In this algorithm, a group of frogs (a set of answers), is divided into several sub branches, where each frog has its own behavior and can obtain the behavior of the other frogs through their evolution [37,38]. Based on this method, in the following, the optimization of the system is discussed. The cost per square meter of a collector is expressed in the following equation [39]:

$$C = M\delta + \frac{RM(t^2 + 2D_i t)}{4W} \quad (38)$$

where M is the cost of fin material per unit material volume, R is ratio of cost per unit volume of tube material to cost per unit volume of fin material. With the combination of the cost function

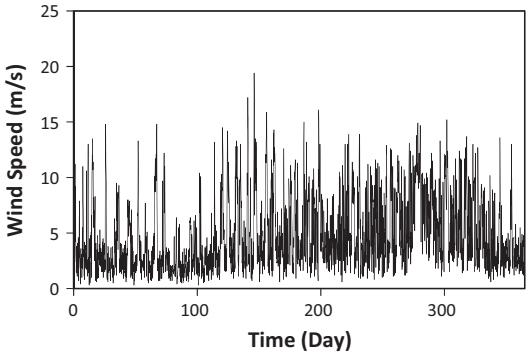

Fig. 9. Wind Profile of Khuznin.

and the equations, described in the previous section, the cost function can be described as:

$$C = \frac{M}{k}\left(\frac{j_o(W - bW^{1/4} - t)^2}{\frac{W - bW^{1/4} - t}{\frac{1}{U_L\left[\frac{1}{F'U_L W} - p\right]}} - 1}\right) + \frac{\pi t^2 RM}{4W} + \frac{2\pi tbRM}{4W^{3/4}} \quad (39)$$

As can be seen, the cost of the system is the function of different parameters and variables. So, the optimization is essential. Also, the parameters of the thermal system are given in Table 3.

4. Results and discussion

For evaluation of the system, firstly, the system is simulated with the conventional dimensions from Table 4. Then, the system

Table 3
Input parameters of the thermal system.

Parameter	Value	Unit
m	400	kg
R	16	kW/K m^2
C_p	4200	J/kg K
A_{tank}	2.5052	m^2
K_{copper}	385	w/m K
K_{water}	0.596	w/m K
L	1	m
ε	0.03	
σ	5.67e−8	J/s m^2 K^4
μ	1e−3	Pa s
T_0	298.15	K

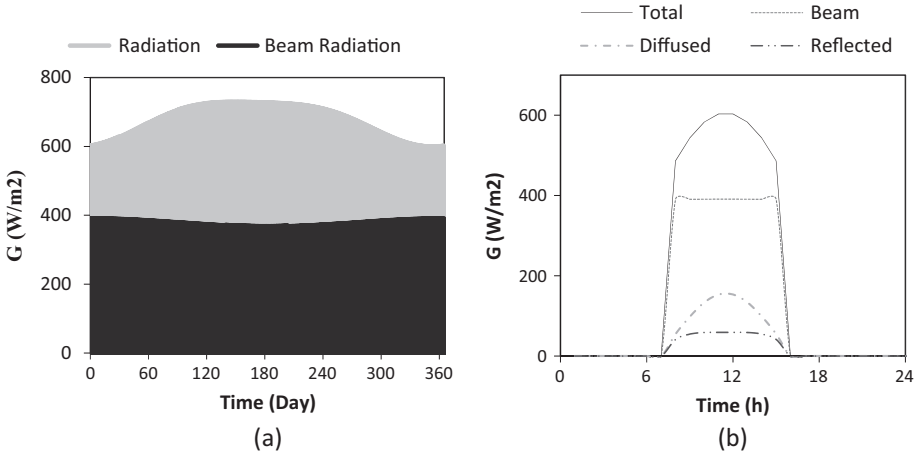

Fig. 8. (a)Total and Beam hourly radiation and (b) fractions of radiation to a dual axis solar tracker.

Table 4
Frog Leap parameters for the optimization of system.

Population size	Chromosome size	Number of memeplex	Number of frogs in each memeplex	Iteration
48	1	4	12	100

is optimized considering the efficiency of the system to be fixed with the minimum cost of the system. So, the thermal characteristics of the system remain the same. The optimization parameters are given in Table 4. In the optimization process the number of selected frogs for each step is equal to 4. The lower amounts reduce the speed of local communication and the higher amounts cause the data not to be properly transferred between memeplexes.

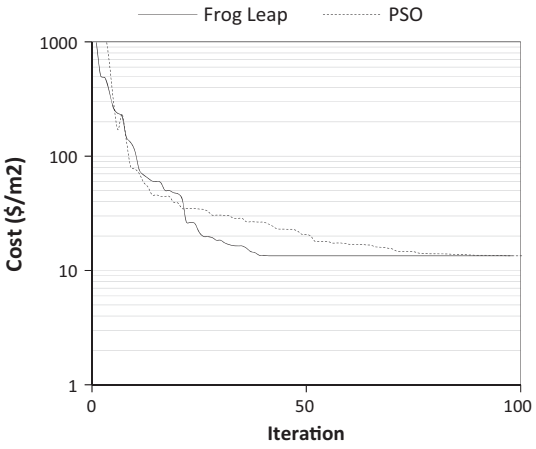

Fig. 10. The convergence of optimization.

Table 5
Optimization results.

Parameter	Optimization result	Conventional dimensions
W	0.06341 m	0.1 m
D_i	0.0045 m	0.0135 m
D_o	0.006 m	0.015 m
δ	5.91e−5 m	5e−4 m
Number of tubes	15	10

Also, the convergence of the Frog Leap is shown in Fig. 10. As it can be seen, the convergence point of the optimization is in the 41st iteration. Also, the particle swarm optimization (PSO) is implemented to the system, which gives the same result in the 84th iteration. The optimization results are shown in Table 5. The optimal calculated cost is 13.44 $/m^2. It should be mentioned, in the optimization procedure, that PV cost is not taken into consideration as PV material will not be optimized due to the fact that the PV is treated as a ready manufactured product on which no changes or modifications whatsoever can be done.

The electrical characteristics of cells of the system are shown in Fig. 11. The maximum voltage and current point are illustrated in the figure. These points give the average efficiency of 37 percent. Also the average fill factor is 0.86.

The average household daily water consumption with 6 consumers is considered 400 liters [40]. The usual consumption time is from 7 a.m. to 12 midnight. So, in the 17 h, the consumption is 23.5 liters per hour. Also, the volume of the tank is considered 300 liters and the amount of pumping of water is 72 liters per hour. The tank is a cylindrical shape with the radius of 0.4 m and the height of 0.596 m.

The results are based on hourly simulation of the system during the year. The absorbed power which produces the electrical and thermal power is shown in Fig. 12a. As can be seen, the fluctuation of power is almost 8 percent, during the year. The average absorbed power is 1200 W which produces average electrical and thermal powers of 450 W, and 575.8 W, respectively. Also, the efficiency of the system is shown in Fig. 12b. Although the radiation and temperature fluctuate during the year, the efficiency of the system remains almost constant at 85 percent with more share of thermal efficiency at an average amount of 47.68 percent. The calculated efficiencies are for the light hours when radiation exists to generate power.

The energy balance of the fluid in the heat storage tank is shown in Fig. 13. As can be seen, the power loss increases with the amount of energy in the tank. The energy loss during the year is 14 MJ which is 0.15 percent of E_{in}. Also, the used energy during the year is 15.5 GJ. As is seen in Fig. 13c. after sunset, when there is not absorbed energy, the energy in the storage tank can satisfy the consumption.

The fluid temperature, shown in Fig. 14, is derived from the energy balance equation and follows the pattern of the collector's temperature. The daily fluctuation of the temperature is caused by the variation of radiation. The lack of radiation and the decrease

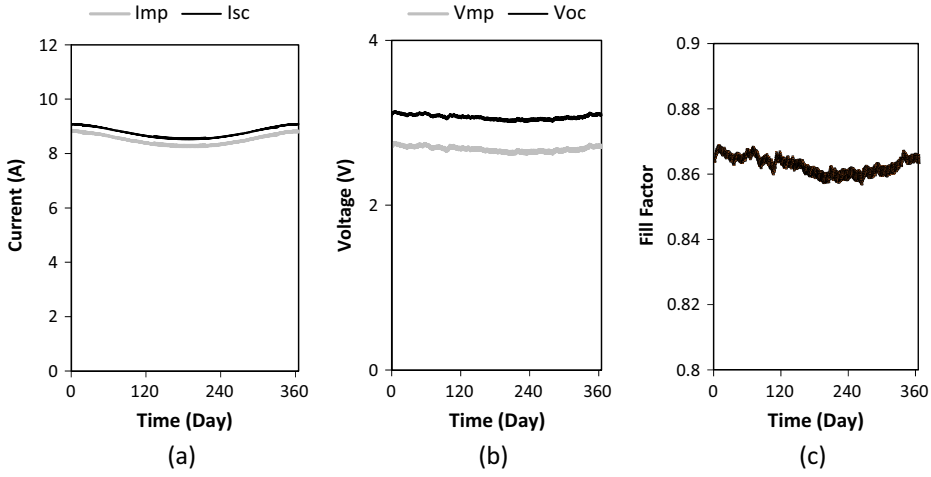

Fig. 11. Electrical characteristics of the system.

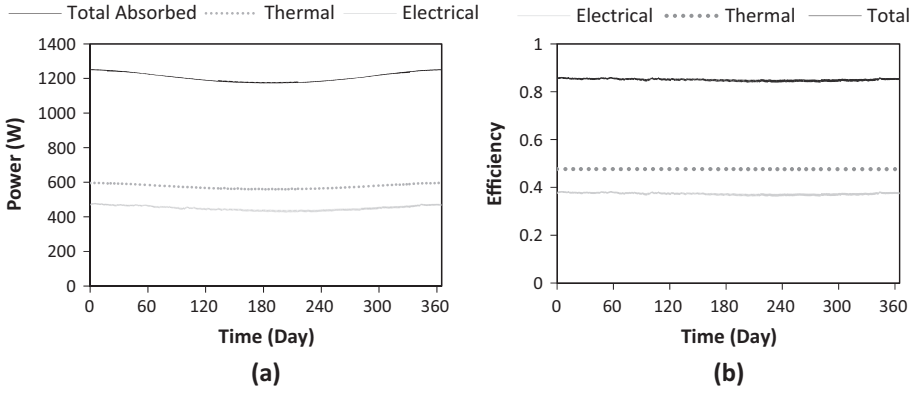

Fig. 12. Power (a) and efficiency (b) of CPVT system.

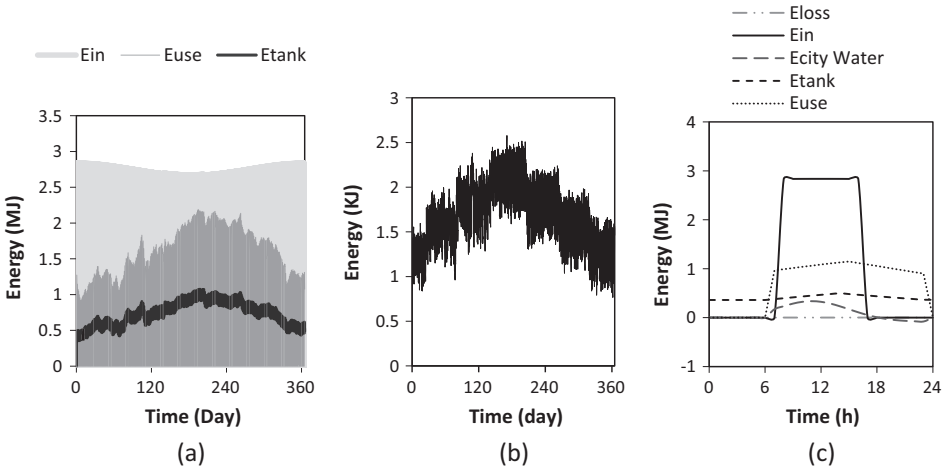

Fig. 13. The Energy balance for the year (a), energy loss (b), and energy balance for the first day (c).

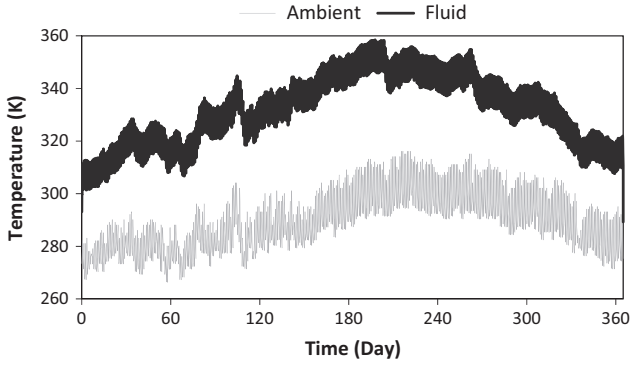

Fig. 14. Fluid Temperature.

of the temperature during night hours cause the decrease of the temperature of the fluid.

The result of the proposed system can be evaluated in comparison with a similar study [41] which is given in Table 6. Both CPVT systems have triple junction cells and concentrated dishes. However, the purpose of that study is to supply the temperature for heating and cooling with changing the number of cells and structure of the system. For this purpose, absorption heat pump (AHP) is used as the cooling system which although it has lower efficacy, water is useless due to demand for high temperature. Although it has a slightly better overall efficiency, it is not desirable because the cost of the PV cell is high and the electrical efficiency is low. In this study, CPVT system is designed in a way that beside the maximum electrical efficiency and minimum cost, the thermal system be utilized with high overall efficiency. It is possible to increase the overall efficiency by lowering the electrical efficacy and raising thermal efficiency, however, it is not the general purpose of a PVT system.

Table 6
Comparison of working condition of Carlo Renno's CPVT with the system proposed in this study.

	This research	Carlo Renno's research
Cell type	Triple-junction	Triple-junction
Manufacturer	BOEING	Unknown
Application	Domestic	Domestic
Configuration	Concentrated dish	Concentrated dish
Absorber configure	Header-riser structure	Single tube structure
Concentration factor	600–800	900
Max. electrical efficiency at work condition	38%	22%
Max. thermal efficiency at work condition	48%	70%
Max. total efficiency at work condition	85%	88%

5. Conclusion

In this study, operation of multi junctional concentrated photovoltaic thermal systems has been simulated and evaluated using the hourly radiation for Qazvin province for a one year period. By designing an active ventilation for the CPVT system, it is concluded that not only the electrical efficiency of the system is increased, but also, the total efficiency is increased to about 85 percent, due to use of generated thermal power. The thermal section of the system is optimized with Frog Leap algorithm to minimize the cost of the system without changing its efficiency, resulting in 13.4 ($/m^2) as the cost of a collector. Also, the simulations show that the temperature of the collector decreases, significantly, with using the heating storage tank. So, active ventilation, besides providing an economic optimization of the system, can improve the issues of the system with regard to passive ventilation and low efficiency.

Finally, it is suggested that in future studies, the optimization of the system be performed with consideration of the grid and the cost of heat generated by fossil fuels. Also, the optimization can be performed prioritizing consumer demand, so that the minimum temperature needed for the consumer is considered as the basis of heat power generation, during a year-long period of operation.

References

[1] Sharaf OZ, Orhan MF. Concentrated photovoltaic thermal (CPVT) solar collector systems: Part II – Implemented systems, performance assessment, and future directions. Renew Sustain Energy Rev 2015;50(C):1566–633.

[2] Marini S, Strada C, Villa M, Berrettoni M, Zerlia T. How solar energy and electrochemical technologies may help developing countries and the environment. Energy Convers Manage 2014;87:1134–40.

[3] Zahedi A. Review of modeling details in relation to low-concentration solar concentrating photovoltaic. Renew Sustain Energy Rev 2011;15:1609–14.

[4] Calise F, d'Accadia MD, Vicidomini M, Scarpellin M. Design and simulation of a prototype of a small-scale solar CHP system based on evacuated flat-plate solar collectors and Organic Rankine Cycle. Energy Convers Manage 2015;90:347–63.

[5] Gafurov T, Usaola J, Prodanovic M. Modelling of concentrating solar power plant for power system reliability studies. IET Renew Power Gener 2015;9 (2):120–30.

[6] Calise F, d'Accadia MD, Roselli C, Sasso M, Tariello F. Desiccant-based AHU interacting with a CPVT collector: simulation of energy and environmental performance. Sol Energy 2014;103:574–94.

[7] Baig Hasan, Sellami Nazmi, Chemisana Daniel, Rosell Joan, Mallick Tapas K. Performance analysis of a dielectric based 3D building integrated concentrating photovoltaic system. Sol Energy 2014;103:525–40.

[8] Xu Z, Kleinstreuer C. Concentration photovoltaic–thermal energy co-generation system using nanofluids for cooling and heating. Energy Convers Manage 2014;87:504–12.

[9] Zhai H, Dai YJ, Wu JY, Wang RZ, Zhang LY. Experimental investigation and analysis on a concentrating solar collector using linear Fresnel lens. Energy Convers Manage 2010;51:48–55.

[10] Chemisana D, Ibanez M, Rossel JI. Characterization of a photovoltaic-thermal module for Fresnel linear concentrator. Energy Convers Manage 2011;52 (10):3234–40.

[11] Vossier A, Chemisana D, Flamant G, Dollet A. Very high fluxes for concentrating photovoltaic: considerations from simple experiments and modeling. Renewable Energy 2012;38:31–9.

[12] Cotal H, Fetzer C, Boisvert J, Kinsey G, King R, Hebert P, et al. IIIeV multijunction solar cells for concentrating photovoltaics. Energy Environ Sci 2009;2:174–92.

[13] Reis F, Brito MC, Corregidor V, Wemans J, Sorasio G. Modeling the performance of low concentration photovoltaic systems. Sol Energy Mater Sol Cells 2010;94 (7):1222–6.

[14] Li M, Li GL, Ji X, Yin F, Xua L. The performance analysis of the trough concentrating solar photovoltaic/thermal system. Energy Convers Manage 2011;52:2378–83.

[15] Bernardo LR, Perers B, Håkansson H, Karlsson B. Performance evaluation of low concentrating photovoltaic/thermal systems: a case study from Sweden. Sol Energy 2011;85(7):1499–510.

[16] Tina GM, Scandura PF. Case study of a grid connected with a battery photovoltaic system: V-trough concentration vs. single-axis tracking. Energy Convers Manage 2012;64:569–78.

[17] Natarajan Sendhil K, Katz M, Ebner R, Weingaertner S, Aßländer O, Cole A, et al. Experimental validation of a heat transfer model for concentrating photovoltaic system. Appl Therm Eng 2012;33:175–82.

[18] Chemisana D, López-Villada J, Coronas A, Ignasi Rosell J, Lodi C. Building integration of concentrating systems for solar cooling applications. Appl Therm Eng 2013;50:1472–9.

[19] Kandilli C. Performance analysis of a novel concentrating photovoltaic combined system. Energy Convers Manage 2013;67:186–96.

[20] Guiqiang L, Gang P, Ming Y, Jie J, Yuehong S. Optical evaluation of a novel static incorporated compound parabolic concentrator with photovoltaic/thermal system and preliminary experiment. Energy Convers Manage 2014;85:204–11.

[21] Hussain MI, Lee GH. Parametric performance analysis of a concentrated photovoltaic co-generation system equipped with a thermal storage tank. Energy Convers Manage 2015;92:215–22.

[22] Hussian M, Lee GH. Experimental and numerical studies of a U-shaped solar energy collector to track the maximum CPV/T system output by varying the flow rate. Energy Convers Manage 2015;76:735–42.

[23] IEC. Specifications of Solar Trackers Used for Photovoltaic Systems. 82/651/DTS: IEC 62727 TS Ed.1, 2012.

[24] Dong Han, Zhichao Wang, Huan Shen, Guili Xu, Fangpei Li. Research and Design on a Rubust Sun-Tracker. In: International Conference on Sustainable Power Generation and Supply, April 2009, p. 1–6.

[25] Lee Chia-Yen, Chou Po-Cheng, Chiang Che-Ming, Lin Ciu-Feng. Sun tracking systems: a review. J Sensors 2009;9:3875–90.

[26] Brogren M, Helgesson A, Karlsson B, Nilsson J, Roos A. Optical properties, durability and system aspects of a new aluminiumpolymer-laminated steel reflector for solar concentrators. Sol Energy Mater Sol Cells 2004;82:387–412.

[27] Wang Z, Zhang H, Wen D, Zhao W, Zhou Z. Characterization of the InGaP/InGaAs/Ge triple-junction solar cell with a two-stage dish-style concentration system. Energy Convers Manage 2013;76:177–84.

[28] Partain LD. Solar cells and their applications. In: 1st ed., Chapter 1, LD Partain, editor. New York, John Wiley & Sons, 1995.

[29] Spectrolab Inc. A Boeing Company. Analytical Model for C1MJ and C3MJ CDO-100 Solar Cells and CCAs. CPV Solar Cell Products. 2009, p. 1–5.

[30] Simon M Sze, Kwok K Ng. Physics of semiconductor devices. In: 2nd ed., 2006. p. 88, eq. 46.

[31] King R, et al. Metamorphic III–V materials, sublattice disorder, and multi-junction solar cell approaches with over 37% cell efficiency. In: Proc 19th European Solar Cell Conf & Exhibition, Paris, France, 2004.

[32] Min Cui, Nuofu Chen, Xiaoli Yang, Yu Wang, Yiming Bai, Xingwang Zhang. Thermal analysis and test for single concentrator solar cells. J Semiconduct 2009;30(4):1–4.

[33] Fox Robert W, Pritchard Philip J, McDonald Alan T. Introduction to fluid mechanics. John Wiley & Sons; 2011. 8th ed.

[34] Duffie, Beckman. Solar engineering of thermal processes. 3rd ed. New York, USA: John Wiley & Sons Inc; 2006.

[35] Kerzmann T, Schaefer L. System simulation of a linear concentrating photovoltaic system with an active cooling system. Renewable Energy 2012;41:254–61.

[36] Gholami H, Khalilnejad A, Gharehpetian GB. Electrothermal performance and environmental effects of optimal photovoltaic-thermal system. Energy Conversion and Management. 2015.

[37] Zhu GY, Zhang WB. An improved Shuffled Frog-leaping Algorithm to optimize component pick-and-place sequencing optimization problem. Expert Syst Appl: Int J 2014;41(15):6818–29.

[38] Lu K, Ting L, Keming W, Hanbing Z, makoto T, Bin Y. An improved shuffled frog-leaping algorithm for flexible job shop scheduling problem. Algorithms 2015;8 (1):19–31.

[39] Charalambous PG, Kalogirou SA, Maidment GG, Yiakoumetti K. Optimization of the photovoltaic thermal (PV/T) collector absorber. Sol Energy 2011;85:871–80.

[40] ASHRAE. ASHRAE handbook: heating, ventilating, and air conditioning applications, inch-pound edition. American Society of Heating Ventilating and Air Conditioning, 2003.

[41] Renno C. Optimization of a concentrating photovoltaic thermal (CPV/T) system used for a domestic application. Appl Therm Eng 2014;67:396–408.